Degradation of 4-aminoantipyrine by electro-oxidation with a boron-doped diamond anode: Optimization by central composite design, oxidation products and toxicity

Lucas de Melo da Silva[a], Fábio Gozzi[a], Ignasi Sirés[b,*], Enric Brillas[b], Silvio Cesar de Oliveira[a], Amilcar Machulek Junior[a,*]

[a] *Institute of Chemistry, Federal University of Mato Grosso do Sul, Av. Senador Filinto Muller, 1555; CP 549, Campo Grande, MS 79074-460, Brazil*
[b] *Laboratori d'Electroquímica dels Materials i del Medi Ambient, Departament de Química Física, Facultat de Química, Universitat de Barcelona, c/Martí i Franquès 1-11, 08028 Barcelona, Spain*

ABSTRACT

Electro-oxidation with electrogenerated H_2O_2 (EO-H_2O_2) was applied to treat acidic aqueous solutions of 4-aminoantipyrine (4-AA), a persistent drug metabolite of dipyrone, in sulfate medium. Trials were made using a boron-doped diamond anode in the presence of H_2O_2 electrogenerated on site. A 2^4 central composite design (CCD) was employed to evaluate the effect of four independent variables, namely current density (j), pH, 4-AA concentration and electrolysis time, on the percentages of degradation and mineralization, as well as on mineralization current efficiency (MCE). Predicted responses agreed with observed values, showing linear trendlines with good R^2 and R^2_{adj} values. The degradation was optimum at $j = 77.5 \, mA \, cm^{-2}$, pH 3.5 and 62.5 $mg \, L^{-1}$ 4-AA, leading to 63% and 99% removal after 3 and 7 min, respectively. For those solutions, the largest mineralization was found at $j = 77.5 \, mA \, cm^{-2}$, attaining 45% abatement at 175 min. Low MCE values were obtained in all electrolyses. An initial route for 4-AA degradation is proposed based on one dimer and eleven aromatic and aliphatic intermediates detected in the treated solutions at pH 3.5 by LC-MS. The initial 62.5 $mg \, L^{-1}$ solution at pH 3.5 presented acute toxicity on *Artemia salina* larvae, with $LC_{50} = 13.6 \, mg \, L^{-1}$, being substantially reduced after 3 and 7 min of EO-H_2O_2 at $j = 77.5 \, mA \, cm^{-2}$ due to the formation of less toxic derivatives.

© 2017.

1. Introduction

Drugs and their metabolites are persistent organic pollutants (POPs) in the aquatic environment since they cannot be removed efficiently in conventional urban wastewater treatment plants (Gómez et al., 2008; Prieto-Rodríguez et al., 2013; Campos-Mañas et al., 2017). They are considered as emerging pollutants, not yet regulated, and their presence as traces in water streams causes great concern because of their potential harmful effects on animals and humans (Brillas and Sirés, 2015; Ebele et al., 2017). Among these chemicals, pyrazolone derivatives like antipyrines and, specially, dipyrone (metamizole) are widely prescribed as analgesics and anti-inflammatory drugs. Up to four metabolites of dipyrone have been detected in sewage treatment systems, being 4-aminoantipyrine (4-AA, $C_{11}H_{13}N_3O$, $M = 203.24 \, g \, mol^{-1}$) predominant with contents ranging between 20 $ng \, L^{-1}$ and 27 $\mu g \, L^{-1}$ (Prieto-Rodríguez et al., 2013; Campos-Mañas et al., 2017). 4-AA exhibits biological activity, is applied to the treatment of viral diseases (Hu et al., 2010) and forms stable complexes with hemoglobin to reduce blood flow (Gowda et al., 2015). However, despite these benefits, pyrazolones are suspect of causing suppression of immune system (i.e., agranulocytosis) (Santos et al., 2010). Several works have reported the degradation of 4-AA by

ozonation (Muñoz et al., 2009) and advanced oxidation processes (AOPs) such as UV/H_2O_2 (Gómez et al., 2008) and photoelectrocatalysis with a TiO_2/ITO anode (Li et al., 2013). AOPs are eco-friendly technologies that involve the generation of reactive oxygen species (ROS) like the strong oxidant hydroxyl radical ($^\bullet OH$), which can destroy many organics including drugs and their metabolites that tend to be resistant to conventional methods (Brillas and Sirés, 2015; Gligorovski et al., 2015; Cavalcante et al., 2016; Da Silva et al., 2016). However, there exists no previous information on the ability of a powerful electrochemical AOP (EAOP) like electro-oxidation (EO) to remove 4-AA from water.

EO is the most common EAOP for wastewater treatment (Panizza and Cerisola, 2009; Feng et al., 2013; Sirés et al., 2014; Moreira et al., 2017). The advantages of this method are simplicity, easy scale-up pre-eminently through modular units, no need of added of chemicals and use of the electron as clean reagent to promote the production of ROS. In EO, a high current density (j) is usually supplied to the electrodes of an electrolytic cell in order to oxidize the water at the anode M, thus producing adsorbed $^\bullet OH$ on its surface (i.e., M($^\bullet OH$)). Nevertheless, the oxidation power of EO depends on the nature of the anode used, since active and non-active anodes behave very differently due to their larger or smaller O_2-evolution overpotential and M-$^\bullet OH$ interaction (Marselli et al., 2003; Guinea et al., 2009; Panizza and Cerisola, 2009; Coria et al., 2016; Steter et al., 2016). In particular, it has been found that boron-doped diamond (BDD) thin-
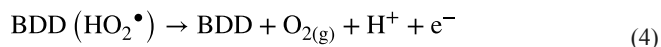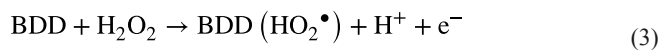
films supported on solid substrates are the best anodes to develop such technology, since they are able to generate large amounts of quasi-free physisorbed BDD($^{\bullet}$OH) from reaction (1) (Boye et al., 2002; Marselli et al., 2003; Özcan et al., 2008; Thiam et al., 2015a, 2015b):

$$BDD + H_2O \rightarrow BDD\left(^{\bullet}OH\right) + H^+ + e^- \tag{1}$$
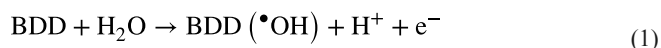
In systems equipped with undivided electrochemical reactors, the nature of the cathode can also play an important role regarding the effectiveness of EO. Organics may undergo reductive transformations on many materials. This can be prevented by using a carbon-polytetra-fluoroethylene (PTFE) air-diffusion electrode since it pre-eminently favors the two-electron reduction of O_2 gas to H_2O_2 from reaction (2) (Sirés et al., 2014). This method is then called EO with electrogenerated H_2O_2 (EO-H_2O_2) (Moreira et al., 2014; Thiam et al., 2015a, 2015b; Guelfi et al., 2017; Lanzalaco et al., 2017), characterized by the oxidation of this species at the BDD anode to yield hydroperoxyl radical via reaction (3), followed by its decomposition to O_2 gas by reaction (4). In EO-H_2O_2, the weak ROS like H_2O_2 and BDD($HO_2^{\bullet}$) can attack the organic pollutants, but to a much smaller extent as compared to BDD($^{\bullet}$OH) (Thiam et al., 2015a, 2015b; Guelfi et al., 2017).

$$O_{2(g)} + 2H^+ + 2e^- \rightarrow H_2O_2 \tag{2}$$

$$BDD + H_2O_2 \rightarrow BDD\left(HO_2^{\bullet}\right) + H^+ + e^- \tag{3}$$

$$BDD\left(HO_2^{\bullet}\right) \rightarrow BDD + O_{2(g)} + H^+ + e^- \tag{4}$$

This work addresses the study of the treatment of 4-AA solutions by means of EO-H_2O_2 using a stirred BDD/air-diffusion tank reactor. The assays were performed according to a 2^4 central composite design (CCD) in order to optimize the treatment upon elucidation of the relationship between j, pH, 4-AA concentration ([4-AA]) and electrolysis time as independent variables. Three responses were considered, namely the degradation and mineralization percentages and the mineralization current efficiency (MCE). Primary intermediates were identified by liquid chromatography-mass spectrometry (LC-MS) and a plausible initial degradation route has been proposed. Finally, the evolution of acute toxicity was determined using the larvae of micro-crustacean *Artemia salina*.

2. Materials and methods

2.1. Reagents

4-Aminoantipyrine (99% purity) was obtained from Sigma-Aldrich. Ultrapure water (Millipore Milli-Q, resistivity >18 MΩ cm at 25 °C) was employed for the preparation of all synthetic 4-AA samples and analytical solutions. Catalase (10,000–50,000 units (mg protein)$^{-1}$) purchased from Sigma-Aldrich was employed to quench generated H_2O_2 before toxicity analysis. Other reagents and solvents were of analytical or HPLC grade supplied by Sigma-Aldrich and Vetec Quimica Fina.

2.2. Electrochemical procedures

The EO-H_2O_2 treatments were carried out with 100 mL of 4-AA solutions containing 0.050 M Na_2SO_4 as background electrolyte. The assays were performed in a one-compartment glass cell that was permanently thermostated by recirculating water at 25 ± 1 °C through a glass jacket. The anode was a BDD thin-film electrode of 3 cm^2 geometric area supplied by NeoCoat (La-Chaux-de-Fonds, Switzerland), synthesized on a single-crystal p-type Si (100) wafer. A cathode with the same geometric area was made from a carbon-PTFE air-diffusion electrode purchased from *E*-TEK (Somerset, NJ, USA). The device was mounted as explained elsewhere (Guelfi et al., 2017) and fed with compressed air at 1 L min^{-1} to continuously electrogenerate H_2O_2. The interelectrode gap was approximately 1 cm. The runs were carried out at constant j provided by a Fa 3003 DC power supply from Instrutherm. Prior to first electrolysis, the electrodes were electrochemically cleaned/activated by polarization in 0.050 M Na_2SO_4 at $j = 100$ mA cm^{-2} for 240 min.

2.3. Analytical methodologies

A Crison 2000 pH-meter was used for pH monitoring during the experiments. All samples were filtered with 0.45 μm PTFE filters from Phenomenex once withdrawn from the solutions. The H_2O_2 content accumulated in the medium was determined from the absorbance of its complex with metavanadate using a Unicam UV–Vis spectrophotometer (Nogueira et al., 2005). The calibration curve for this method obeyed the Beer's law within the 0.2–2000 mg L^{-1} range. The concentration of NH_4^+ and NO_3^- ions in treated solutions was determined from the standard methods SM4500-NH_3 C (titrimetric method) and SM 4500-NO_3^- E, respectively (APHA, 2012).

Reversed-phase HPLC analysis of solutions for monitoring 4-AA concentration decay was performed with a Finnigan Surveyor system from Thermo Scientific, using a Zorbax Eclipse XDB-C-18 5 μm (250 mm × 4.6 mm) column from Agilent Technologies and the detector set at 274 nm. Aliquots of 25 μL were injected into the above system and elution was ensured with a 60:40 (v/v) methanol/water mixture at 0.5 mL min^{-1} as mobile phase. Each aliquot was previously diluted sample with acetonitrile 1:1 (v/v). The chromatograms exhibited a good peak for 4-AA at retention time of 6.5 min and its concentration was obtained with LOD = 0.025 mg L^{-1}.

The mineralization attained upon electrolysis of solutions was followed from the decay of their total organic carbon (TOC). This was determined by injecting fresh 50 μL aliquots into a Shimadzu TOC VCPN analyzer. TOC values with ±2% accuracy, LOQ = 0.180 mg L^{-1} and LOD = 0.053 mg L^{-1} were obtained.

For the identification of intermediates by LC-MS, mixtures of 5 mL of sample and methanol were prepared and 1 μL was injected into an LC-20AD system from Shimadzu with a Kinetex C18 100A 2.6 μm (150 mm × 2.1 mm) column at 50 °C and coupled to an IES-Q-QTOF microTOFIII detector from Bruker Daltonics. It operated in positive electrospray ionization mode at spray voltage of 0.8–1.2 V and capillary voltage of 3500 V, at 200 °C. The spectra were acquired within the *m/z* 120–1300 range. Gradient elution with water (phase A) and acetonitrile (phase B), both with 0.1% formic acid, at a flow rate of 0.3 mL min^{-1} was employed as follows: 0–2 min, from 0% to 3% B; 2–25 min, from 3% to 25% B; 25–40 min from 25% to 80% B; and 40–48 min, from 80% to 3% B.

The acute toxicity tests were carried out with larvae of microcrustacean *Artemia salina* after hatching of the cystic in synthetic seawater at 32 g L^{-1}, pH 8–9 under aeration for 48 h. Tests were performed

in duplicate (5 individuals per replicate) at $20 \pm 2\,°C$ in well cell culture plates of 3 mL, with a photoperiod of 16 h light and 8 h dark for 96 h in a static system. The dead larvae were counted to obtain median lethal concentrations (LC_{50}), i.e., the concentrations that killed 50% of larvae within 96 h of exposure, which were calculated from five dilutions (70, 50, 25, 12.5 and 6.25% v/v) (Da Silva et al., 2016; El Fels et al., 2016).

2.4. Central composite design

A CCD modeling based on response surface methodology (RSM) was utilized to assess the effect of independent variables on different parameters that are directly related to the performance of $EO-H_2O_2$ to remove 4-AA: percentages of degradation and mineralization, and MCE. Four independent variables were selected to model each response, namely j (X_1), pH (X_2), initial [4-AA] (X_3) and electrolysis time (X_4). Twenty-seven experiments with a 2^4 factorial design using 16 cube points, 8 axial points and one triplicate at the center point were devised. The experimental matrix was generated using Statistica

10 software (StatSoft, Tulsa, USA). Table 1 summarizes the experimental ranges and levels of the four independent variables chosen to evaluate the $EO-H_2O_2$ process. Note that two different time ranges were used to evaluate the three dependent parameters.

From the results obtained using the above 2^4 CCD methodology and based on the corresponding RSM analysis, second-order polynomial equations were developed to describe the interaction between the dependent response and the independent (linear and quadratic) variables (Kasiri and Khata, 2011; Da Silva et al., 2016), as follows:

$$Y = \beta_0 + \sum_{i=1}^{k} \beta_i X_i + \sum_{1 \leq i < j}^{k} \beta_{ij} X_i X_j + \sum_{i=1}^{k} \beta_{ii} X_i^2 \tag{5}$$

where k denotes the number of independent variables (=4), Y represents the dependent variable (% degradation, % mineralization or MCE), β_0 is a constant, and β_i, β_{ii} and β_{ij} denote the regression coefficients for the linear X_i, quadratic X_i^2 and interaction $X_i X_j$ terms (X_i, X_i^2 and $X_i X_j$ are the coded experimental levels of the independent variables), respectively.

3. Results and discussion

3.1. Factorial design: removal of 4-AA and TOC abatement

Table 2 summarizes the observed percentages of degradation and mineralization obtained for the 27 experiments designed according to the levels chosen for the independent variables (Table 1). Predicted responses by CCD for both parameters summarized in Table 2 were generated as arithmetic averages with confidence limits of ±95%, and are shown in Fig. 1a for the percentage of degradation and Fig. 1c for the percentage of mineralization. Correlation coefficients (R^2) and ad-

Table 1
Levels of the independent variables used for the 2^4 central composite design with added center point developed for the $EO-H_2O_2$ process of 100 mL of 4-AA solutions in 0.050 M Na_2SO_4.

Independent variable	Level				
	−2	−1	0	+1	+2
Current density (mA cm^{-2})	10.0	32.5	55.0	77.5	100.0
pH	1.0	3.5	6.0	8.5	11.0
[4-AA] (mg L^{-1})	25.0	62.5	100.0	137.5	175.0
Time for % 4-AA degradation (min)	1	3	5	7	9
Time for % 4-AA mineralization and for MCE (min)	10	65	120	175	230

Table 2
Observed and predicted values for the percentages of 4-AA degradation and mineralization and for MCE obtained for the $EO-H_2O_2$ treatment of 100 mL of 4-AA solutions in 0.050 M Na_2SO_4 using different combinations of the 2^4 CCD.

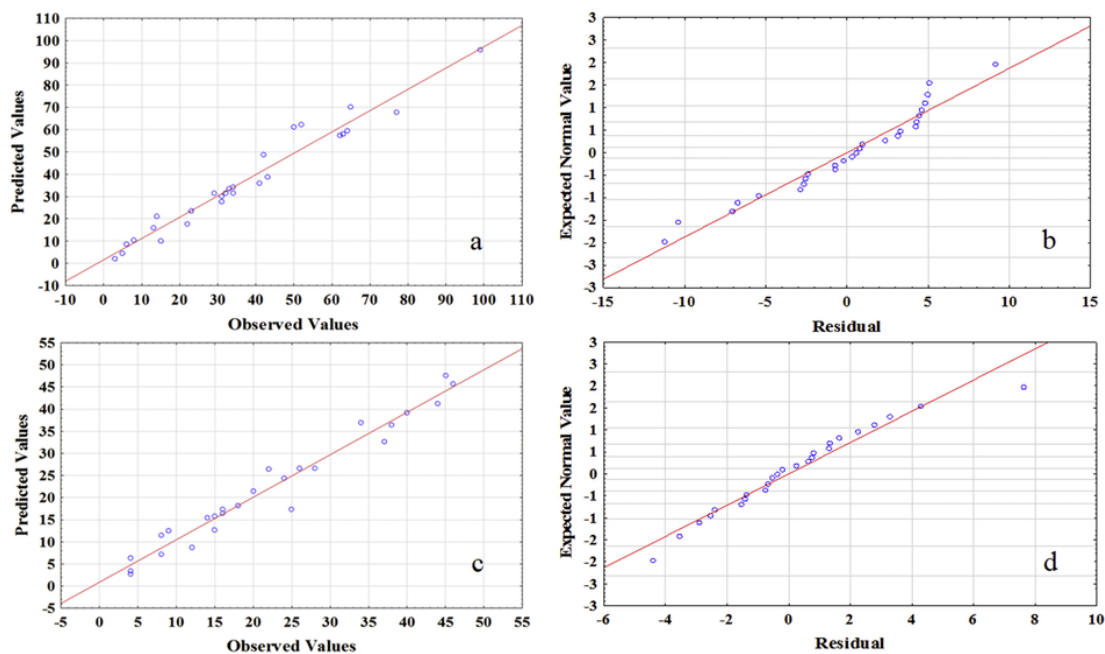| Experiment	Current density (mA cm^{-2})	pH	[4-AA] (mg L^{-1})	Time for degradation (min)	Time for mineralization and for MCE (min)	% 4-AA degradation		% 4-AA mineralization		MCE (%)	
						Observed	Predicted	Observed	Predicted	Observed	Predicted
1	32.5	3.5	62.5	3	65	31	27.9	8	11.5	8.0	8.6
2	32.5	3.5	62.5	7	175	64	59.5	22	26.4	5.9	7.0
3	32.5	3.5	137.5	3	65	6	8.5	4	6.4	5.3	5.3
4	32.5	3.5	137.5	7	175	41	36.2	16	16.5	10.0	9.7
5	32.5	8.5	62.5	3	65	14	21.0	8	7.3	3.6	4.4
6	32.5	8.5	62.5	7	175	43	38.7	24	24.4	2.3	1.4
7	32.5	8.5	137.5	3	65	3	2.2	4	3.4	1.2	3.7
8	32.5	8.5	137.5	7	175	13	15.9	15	15.8	7.6	6.3
9	77.5	3.5	62.5	3	65	63	58.0	20	21.4	1.5	3.3
10	77.5	3.5	62.5	7	175	99	95.7	45	47.5	2.1	0.3
11	77.5	3.5	137.5	3	65	34	34.2	14	15.5	5.2	5.0
12	77.5	3.5	137.5	7	175	77	67.9	34	36.9	6.1	5.8
13	77.5	8.5	62.5	3	65	33	33.7	16	17.4	2.9	3.9
14	77.5	8.5	62.5	7	175	62	57.4	46	45.8	2.9	1.3
15	77.5	8.5	137.5	3	65	8	10.4	15	12.8	6.7	6.0
16	77.5	8.5	137.5	7	175	31	30.0	38	36.4	7.2	7.3
17	10	6.0	100	5	120	5	4.4	12	15.9	12.4	10.4
18	100	6.0	100	5	120	42	45.6	40	39.0	4.0	5.7
19	55	1.0	100	5	120	52	58.1	25	21.7	5.1	4.4
20	55	11.0	100	5	120	22	19.3	9	15.7	1.7	1.9
21	55	6.0	25	5	120	65	66.5	37	36.8	1.7	1.9
22	55	6.0	175	5	120	23	25.8	18	22.4	6.2	5.4
23	55	6.0	100	1	10	15	10.2	4	4.5	10.6	7.1
24	55	6.0	100	9	230	50	58.5	44	49.7	4.8	6.4
25	55	6.0	100	5	120	32	30.0	28	27.6	5.4	6.3
26	55	6.0	100	5	120	34	30.0	26	27.6	5.1	6.3
27	55	6.0	100	5	120	29	30.0	26	27.6	5.1	6.3

Fig. 1. Comparison of predicted and observed values for the percentage of: (a) 4-AA degradation and (c) 4-AA mineralization. Residual plots for the responses of the percentages of: (b) 4-AA degradation and (d) 4-AA mineralization.

justed correlation coefficients (R^2_{adj}) were determined from the observed and predicted values, respectively. Both sets of values were quite similar, exhibiting a very good linear relationship (see Fig. 1a and c), with $R^2 = 0.956$ and $R^2_{adj} = 0.905$ for the percentage of 4-AA degradation and $R^2 = 0.959$ and $R^2_{adj} = 0.913$ for the percentage of 4-AA mineralization. Based in the good agreements between the experimental and predicted values, it can be concluded that the model was satisfactory (Kasiri and Khata, 2011; Da Silva et al., 2016).

Fig. 1b and d shows the excellent linear correlations obtained between the corresponding expected normal values and the residuals (i.e., the difference between the predicted and observed values, corresponding to variation elements unexplained by the fitted model). As can be seen, the two mathematical models were robust, yielding close values to the experimental data and thus providing low residual values that are expected to follow a normal distribution, being independent between them (Bezerra et al., 2008; Kasiri and Khata, 2011; Da Silva et al., 2016). Therefore, the proposed models for the observed sets of experimental data were suitable to describe both responses (Savic et al., 2014; Da Silva et al., 2016).

3.1.1. Percentage of 4-AA degradation

Fig. 2a shows the Pareto chart for the percentage of degradation, revealing that the four linear independent variables, as well as a quadratic initial drug concentration, were statistically significant with $p < 0.05$. Furthermore, the interaction between j and pH (1Lby2L term) was also significant. Fig. 2b exemplifies the response surface generated for the percentage of 4-AA degradation vs. pH and j treating 62.5 mg L^{-1} drug for 3 min.

Fig. 2b depicts that at pH 8.5, the current density did not exert a great effect on 4-AA degradation, as demonstrated by similar values of drug removal at lower and higher j values. In contrast, at pH 3.5, a gradually higher j caused a larger degradation. For example, 63% degradation was achieved at $j = 77.5$ mA cm^{-2}, being much >31% obtained at $j = 32.5$ mA cm^{-2}. Increasing j usually leads to a higher rate of all electrochemical reactions. This is confirmed for 4-AA at

pH 3.5, producing a faster direct oxidation of the drug at the anode and the production of larger amounts of BDD($^{\bullet}$OH) and H_2O_2 via reactions (1) and (2), respectively, thereby enhancing its removal. From Table 2, it can be seen that 99% of 4-AA removal could be attained after only 7 min at $j = 77.5$ mA cm^{-2}.

It is evident that the treatment at acidic pH showed a much better performance regarding the 4-AA degradation as compared to that in alkaline medium. To explain this effect, the amount of H_2O_2 accumulated in the bulk was determined under the above optimum conditions. About 5.2 and 2.5 mM H_2O_2 were found after 7 min of EO-H_2O_2 treatment of 62.5 mg L^{-1} drug at $j = 77.5$ mA cm^{-2} at pH 3.5 and 8.5, respectively. This behavior suggests a much larger consumption of H_2O_2 at pH = 8.5, which can be related to fast reactions of BDD($HO_2^{\bullet}$) formed from reaction (3) with oxidation products of 4-AA. These reactions compete with the direct anodic oxidation of the parent pollutant at the anode and its attack by BDD($^{\bullet}$OH), thus decelerating the drug removal.

The signs of the estimated regression coefficients account for the effect of the independent variables on the treatment. Therefore, positive coefficients inform about a larger degradation upon increase of the given variable value within the range tested. Conversely, negative coefficients indicate a better performance when the value of the variable is diminished. The interaction variables $X_i X_j$ cause a synergistic or antagonistic influence if they are accompanied by positive or negative coefficients, respectively (Nogueira et al., 2005; Calza et al., 2013; Da Silva et al., 2016).

The quadratic model generated for the percentage of 4-AA degradation is given by Eq. (6):

$$Y \ (\%\text{degr.}) = 31.67 + 22.17X_1 - 22.3X_2 - 23.3X_3 + 7.7X_3^2 + 25.67X_4 - 8.8X_1X_2 \quad (6)$$

where X_i denote the levels of the independent variables (see subSection 2.4). Apart from the linear variables, Eq. (6) shows that
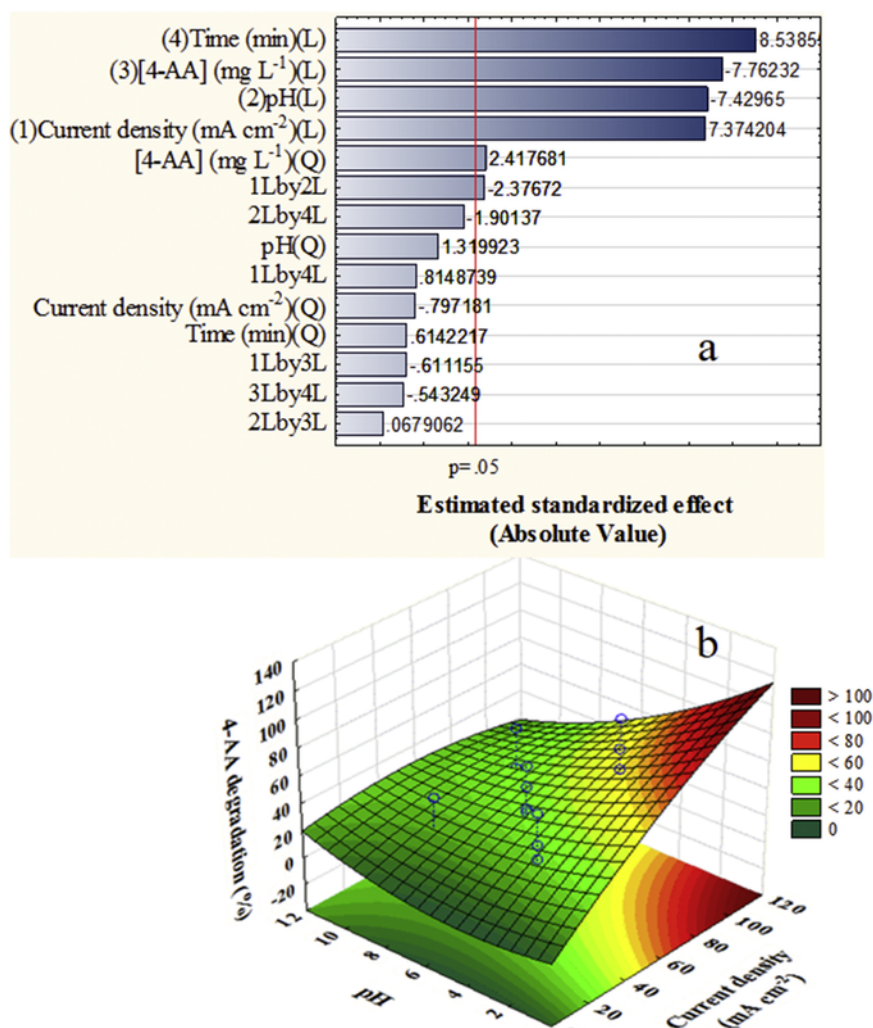
Fig. 2. (a) Pareto chart for the percentage of 4-AA degradation. (b) Response surface plot for such percentage of degradation vs. current density and pH, upon EO-H$_2$O$_2$ treatment of solutions with 62.5 mg L^{-1} drug for 3 min.

the quadratic variable X_3^2 and the interaction X_1X_2 term have an important influence on the response.

Positive coefficients can be observed in Eq. (6) for j and electrolysis time, which reveals an enhancement of the percentage of degradation when these variables adopt higher values. Nevertheless, it must be taken into account that the rise in current is expected to decrease the efficiency of the process due to the acceleration of parasitic reactions of BDD($^{\bullet}$OH), causing a larger production of O$_2$ gas as a first collateral effect, along with an enhancement of H$_2$ evolution at the cathode from water reduction (Sirés et al., 2014; Brillas and Sirés, 2015; Benito et al., 2017). The positive influence of electrolysis time is logical since longer time tends to favor the gradual oxidation of drug molecules. The negative coefficient for pH indicates a quicker degradation as the solution becomes more acid, also associated with the production of more H$_2$O$_2$, as pointed out above. The fact that 4-AA concentration was accompanied by a negative coefficient in Eq. (6) can be simply associated with the quicker removal of lower amounts of molecules under similar oxidative, since a steady concentration of oxidants can deal better with a limited number of drug molecules present in the medium (Sirés et al., 2014; Brillas and Sirés, 2015). In contrast, the quadratic 4-AA concentration showed a smaller but positive coefficient, as expected if its rise enhanced the

degradation efficiency, according to the prediction of a rotatability model (Brereton, 2003; Singh et al., 2004). Note that the negative relationship between j and pH (X_1X_2 term in Eq. (6)) revealed an antagonistic effect on the degradation and then, similar percentages of degradation can be achieved with an opposite change of both variables. For example, after 3 min of treatment of 62.5 mg L^{-1} 4-AA, 31% degradation was reached at $j = 32.5$ mA cm^{-2} and pH = 3.5, exhibiting close value at $j = 77.5$ mA cm^{-2} and pH = 8.5 with 33% 4-AA degradation. Consequently, the interaction effects between the independent variables are of extreme importance to predict the observed percentages of 4-AA degradation using CCD.

3.1.2. Percentage of 4-AA mineralization

The Pareto chart of Fig. 3a evidences the statistical significance ($p < 0.05$) of j, initial drug concentration, electrolysis time, quadratic variable pH and the relationship between j and time (1Lby4L term) to describe the behavior of the percentage of 4-AA mineralization. The response surface of this latter parameter against j and time for EO-H$_2$O$_2$ treatments of 62.5 mg L^{-1} 4-AA at pH = 3.5 is presented in Fig. 3b. No significant influence of pH on the mineralization rates was found, in agreement with similar treatments of other organics (Moreira et al., 2017). It is worth remarking that high j values and
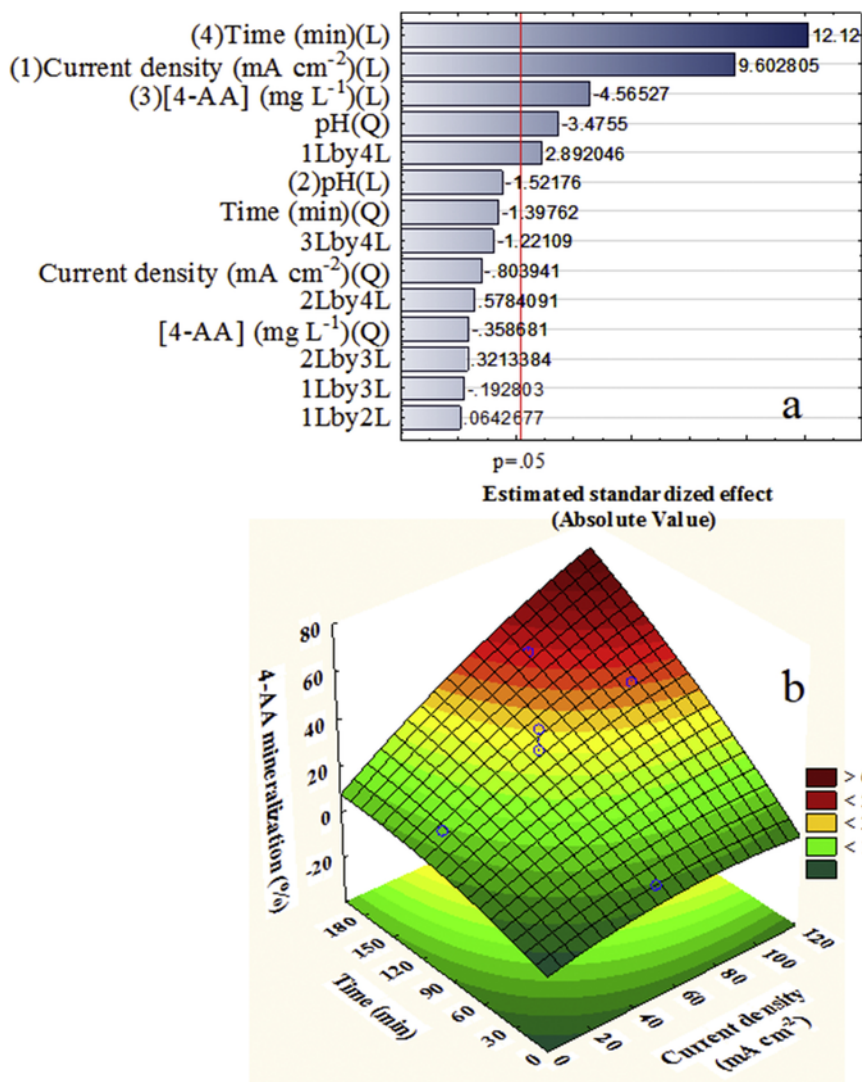
Fig. 3. (a) Pareto chart for the percentage of 4-AA mineralization. (b) Response surface plot for the percentage of mineralization vs. current density and time, upon EO-H$_2$O$_2$ treatment of solutions with 62.5 mg L^{-1} drug at pH=3.5.

long times were required to attain a relatively large mineralization. For example, under the optimum conditions found above for the 4-AA degradation (j=77.5 mA cm^{-2}, pH=3.5 and 62.5 mg L^{-1} drug), only 45% mineralization was reached after 175 min. Prolonging the treatment until 510 min, an almost total mineralization with 91% TOC abatement was already achieved, indicating that ROS (mainly BDD($^\bullet$OH)) originated in the EO-H$_2$O$_2$ process are able to destroy most of the products formed from 4-AA oxidation (Rabaaoui et al., 2013; Moreira et al., 2017).

The estimated regression coefficients allowed generating the following empirical model as response for the percentage of 4-AA mineralization:

$$Y \text{ (\%miner.)} = 26.67 + 15.25X_1 - 7.25X_3 \\ + 19.25X_4 - 5.85X_2^2 + 5.63X_1X_4 \qquad (7)$$

where X_i correspond to the same variables cited above, and X_1X_4 represents the interaction term between j and time.

The positive coefficients of j and time in Eq. (7) represent an improvement of mineralization with the increase of their values. The small positive coefficient for the relationship between j and time (X_1X_4 term) highlights a synergistic effect since a simultaneous increase of their values enhances the TOC removal. This can be deduced from the behavior found for 62.5 mg L^{-1} drug at pH=3.5, where TOC was reduced by 8% and 22% after 65 and 175 min at j=32.5 mA cm^{-2}, respectively, whereas it increased to 45% after 175 min at j=77.5 mA cm^{-2}. On the other hand, the 4-AA concentration exhibited a negative coefficient, as expected if the mineralization was favored at lower drug content owing to the smaller amount of organic matter to be mineralized with the steady concentration of oxidants (Sirés et al., 2014; Brillas and Sirés, 2015).

The quadratic variable pH exhibited a negative coefficient. Thus, in this model the quadratic variable can be reduced, demonstrating still efficiency in the prediction for the model based on rotatability (Brereton, 2003; Singh et al., 2004).

3.1.3. Mineralization current efficiency

The inorganic nitrogenated ions released from the N atoms (0.732 mM) present in a 50 mg L^{-1} 4-AA solution with 0.050 M Na$_2$SO$_4$ at pH = 3 upon EO-H$_2$O$_2$ treatment were analyzed after 210 min of electrolysis at $j = 80$ mA cm^{-2}. Concentrations of 0.26 mM of NO$_3^-$ ion (8.0% of initial N) and 0.82 mM of NH$_4^+$ ion (87.1% of initial N) were obtained. These results revealed the mineralization of 95.1% of initial N, suggesting that the rest of N either remained in the final solution as N-derivatives or was partly lost as volatile species such as N$_2$ and N$_x$O$_y$ (Sirés et al., 2014; Moreira et al., 2017). From these findings, the following theoretical reaction can be proposed for 4-AA mineralization with formation of NH$_4^+$ as pre-eminent ion and a number of electrons (n) equal to 46:

$$C_{11}H_{13}N_3O + 21H_2O \rightarrow 11CO_2 + 3NH_4^+ + 43H^+ + 46e^- \tag{8}$$
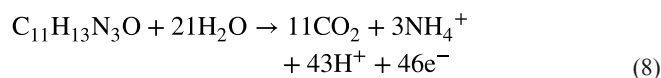
Considering $\Delta(TOC)_{exp}$ as the decay in experimental TOC (in mg L^{-1}) obtained for the different assays, the dependent variable MCE was calculated at each current I (in A) and electrolysis time t (in h) as follows (Sirés et al., 2014; Steter et al., 2016):

$$MCE \ (\%) = \frac{n \, F \, V_s \, \Delta(TOC)_{exp}}{4.32 \times 10^7 m \, I \, t} 100 \tag{9}$$

where F is the Faraday constant, V_s is the solution volume (in L), 4.32×10^7 is a factor to homogenize units and $m = 11$ is the number of carbon atoms of 4-AA.

The MCE values determined from Eq. (9) and listed in Table 2 were small ($\leq 12.4\%$), as a result of the large recalcitrance of intermediates generated. Fig. 4a presents the Pareto chart related to MCE, showing that only j, initial [4-AA] and the relationship between j and pH (1Lby2L term) were statistically significant ($p < 0.05$). The response surface plot for this parameter against j and pH for the treatment of 62.5 mg L^{-1} drug for 65 min is shown in Fig. 4b. It should be noted that Eq. (9) reveals that I (or j) and time are inversely proportional to MCE and hence, their increase causes a decrease of this parameter. In contrast, MCE depends directly on $\Delta(TOC)_{exp}$ at any given electrolysis time. Optimum mineralization conditions were found at a low $j = 32.5$ mA cm^{-2}, with MCE values of 8% at pH = 3.5 and 3.6% at pH = 8.5 after 65 min of treatment. At the same electrolysis time, a higher $j = 77.5$ mA cm^{-2} yielded lower MCE values of 1.5% and 2.9%.

Eq. (10) gives the quadratic model generated by CCD for MCE as a function of the levels of X_1 and X_3 related to the variables j and initial 4-AA concentration, respectively:
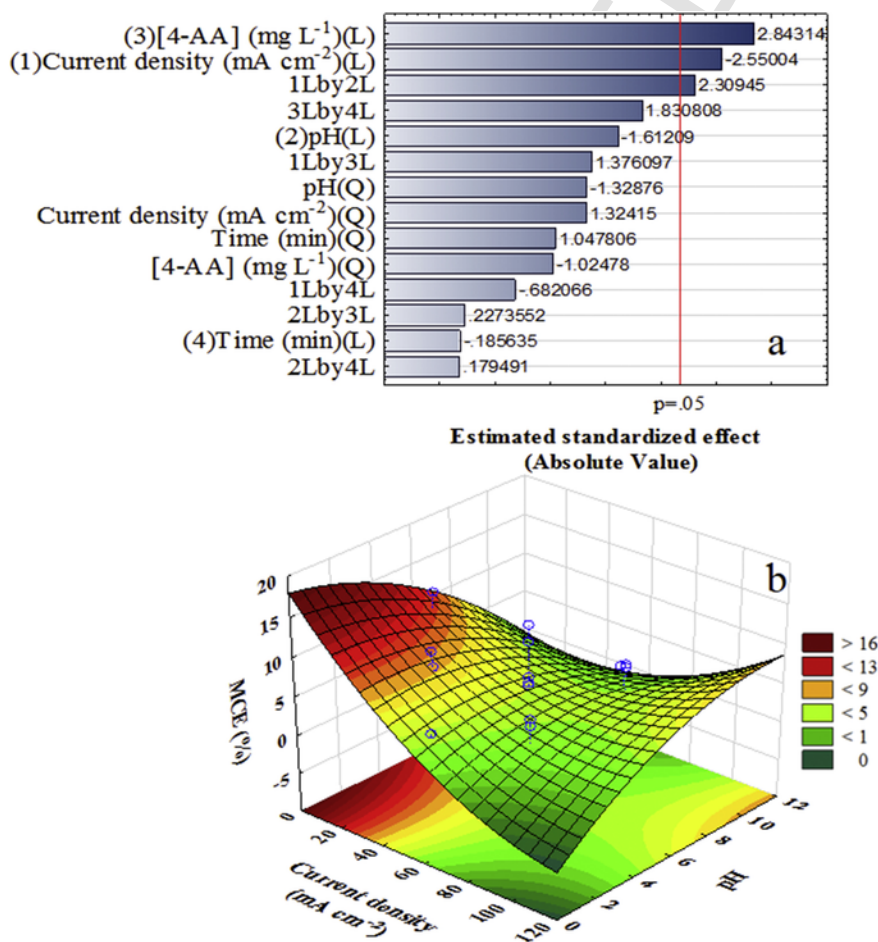

Fig. 4. (a) Pareto chart for MCE and (b) response surface plot of MCE vs. current density and pH, upon EO-H$_2$O$_2$ treatment of solutions with 62.5 mg L^{-1} drug for 65 min.

$$Y \ (\text{MCE}) = 5.2 - 2.18X_1 + 2.43X_3 + 2.41X_1X_2 \qquad (10)$$

where X_1X_2 denotes the interaction term between j and pH.

The negative coefficient of j predicts that its rise causes a decay of MCE, whereas the positive coefficient of [4-AA] is related to an enhancement of MCE at higher organic matter content owing to the direct relationship of this response with $\Delta(\text{TOC})_{exp}$. The synergistic effect of the interaction between j and pH presupposes that the simultaneous decrease of both variables yields the same effect over MCE. For example, for 62.5 mg L^{-1} 4-AA solutions treated for 65 min gave 2.9% MCE at $j = 77.5$ mA cm^{-2} and pH 8.5, which increased to 8% MCE by decreasing j to 32.5 mA cm^{-2} and pH to 3.5, attaining close $\Delta(\text{TOC})_{exp}$ values of 8 and 9 mg L^{-1}, respectively. This confirms that the mineralization current efficiency of the process is strongly related to the applied j value.

3.2. Detection of primary intermediates and proposed initial reaction pathway

The primary oxidation products of 4-AA (**1**) were determined by LC-MS analysis of the final solutions obtained upon EO-H$_2$O$_2$ treatment of a 62.5 mg L^{-1} drug solution in 0.050 M Na$_2$SO$_4$ at pH = 3.5 and $j = 77.5$ mA cm^{-2}, after 3 and 7 min of electrolysis Molecular peaks of 11 [M+H]$^+$ species with m/z values ranging between 164 and 272 were identified, along with one peak of m/z 440 corresponding to a dimer derivative. The major part of these primary products were hydroxylated and carboxylic acid derivatives arising from the attack of BDD($^\bullet$OH) onto the pyrazolone ring of 4-AA. From these findings, Fig. 5 shows a proposed reaction pathway for the initial
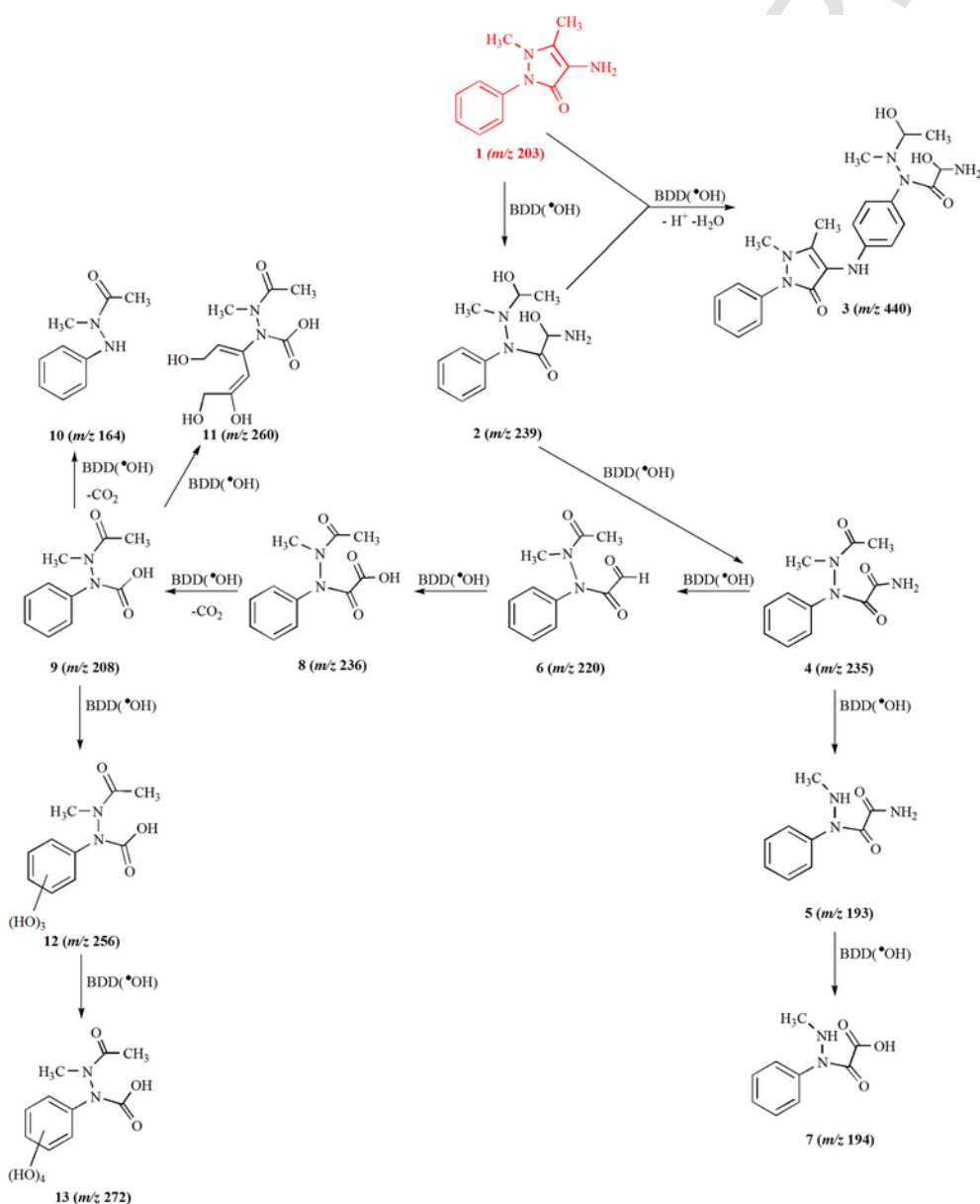

Fig. 5. Proposed reaction pathway for the initial degradation of 4-AA by EO-H$_2$O$_2$ treatment at pH = 3.5.

degradation of 4-AA by this electrochemical AOP where the above radical was assumed as the main oxidant, although slower parallel oxidation with other ROS (e.g., H_2O_2 and $HO_2^{\bullet}$) is feasible as well. Note that the compounds with m/z 164, 220, 235, 236 and 260 have been previously reported using photodegradation, ozonation, Fenton and photo-Fenton for 4-AA treatment (Pérez-Estrada et al., 2007; Gómez et al., 2008; Giri and Golder, 2015; Miao et al., 2015a, 2015b).

The route is initiated by the hydroxylation of **1** (m/z 203) with the cleavage of the C(3)-C(4) bond of the pyrazolone ring to yield **2** (m/z 239). This compound undergoes either dimerization with **1** to form **3** (m/z 440) or oxidation to derivative **4** (m/z 235) that contains three carbonyl groups due to the simultaneous transformation of the alcohol groups of **2**. Fig. 6 schematizes the mechanism proposed for the generation of dimer **3**, involving the oxidation of the –NH_2 group of the pyrazolone ring of **1** by direct charge transfer to the BDD anode to give its radical cation $1^{+\bullet}$ (Hu et al., 2010; Benito et al., 2017). Note that this kind of radical cation may also be formed upon action of BDD($^{\bullet}$OH), as was proposed to explain the demethylation of 4-(N,N-dimethyl)-aminoantipyrine (Santos et al., 2010). This radical then attacks the C(4) of the benzene ring of **2** via BDD($^{\bullet}$OH) oxidation with deprotonation and water formation to form the dimer **3**. Fig. 5 also shows that subsequent deacetylation or deamination of the amide group of **4** leads to the formation of **5** (m/z 193) or **6** (m/z 220), respectively. Compound **5** then undergoes deamination due to hydroxylation, with formation of the carboxylic acid **7** (m/z 194), whereas compound **6** is consecutively oxidized to originate the carboxylic acid product **8** (m/z 236) and decarboxylated to yield **9** (m/z 208). Finally, compound **9** is further decarboxylated to **10** (m/z 164), undergoes a multiple hydroxylation with cleavage of the benzenic ring to form the aliphatic carboxylic acid **11** (m/z 260), or the benzene moiety is trihydroxylated to **12** (m/z 256), which is subsequently hydroxylated to **13** (m/z 272). Note that hydroxylation of the aromatic ring has also been found to be a main degradation route in the case of other aminoantipyirines (Santos et al., 2010).

The mineralization process followed by the primary products is much longer than 4-AA removal because many intermediates react very slowly with BDD($^{\bullet}$OH), such as the final short-chain aliphatic carboxylic acids expected to be formed from the breaking of the benzene ring of the molecule upon hydroxylation (Feng et al., 2013; Sirés et al., 2014; Moreira et al., 2017). This is supported by the fact that up to 510 min were required to reach 91% mineralization of the

62.5 mg L^{-1} solution at pH=3.5 and j=77.5 mA cm^{-2}, a time much longer than 7 min needed to remove the parent drug.

3.3. Acute toxicity to Artemia salina

The assessment of the toxicity of by-products generated by AOPs compared to the initial organic pollutants is crucial, aiming to shorten the duration of expensive treatment and combine them with low cost processes. To do this, the larvae of microcrustacean *Artemia salina* have been widely used because they are easy to handle and show an acute toxicity response to persistent pollutants (Marković et al., 2015; Da Silva et al., 2016). This organism was then employed to evaluate the toxicity of the initial 62.5 mg L^{-1} 4-AA solution at pH=3.5, as well as that of the solutions treated for 3 and 7 min by EO-H_2O_2 at j=77.5 mA cm^{-2}, where 63% and 99% of 4-AA degradation were achieved, respectively. The residual H_2O_2 was removed by adding 1 g L^{-1} catalase solution dropwise.

Fig. 7 highlights the variation of the larvae mortality with the concentration of diluted samples prepared with each of the three tested solutions, as described in subSection 2.3. A greater mortality with increasing 4-AA concentration was found for the parent solution, which allowed determining a LC$_{50}$ value of 13.6 mg L^{-1}. This corresponds to 7.4 acute toxicity units (TU$_a$=(1/LC$_{50}$)×100), which is within the range of 1–10 that informs about a highly toxic chemical (Persoone et al., 2003). In contrast, the solutions treated by EO-H_2O_2 did not show any remarkable acute toxicity since larvae mortality was similar to that found for control samples, thus preventing the determination of their LC$_{50}$ values (Persoone et al., 2003). These findings reveal the non-toxic nature of hydroxylated and carboxylic acids products formed from this treatment (see Section 3.2), in agreement with results reported for the degradation of other drugs (Cavalcante et al., 2015; Marković et al., 2015; Tay and Madehi, 2015; Da Silva et al., 2016).

4. Conclusions

It has been shown that a 2^4 CCD is able to correctly assess the effect of the main independent variables on the EO-H_2O_2 treatment of 4-AA solutions with a stirred BDD/air-diffusion cell. Current density, 4-AA concentration and electrolysis time had an important role regarding the percentages of degradation and mineralization and the MCE. In contrast, the solution pH did not show significant influence
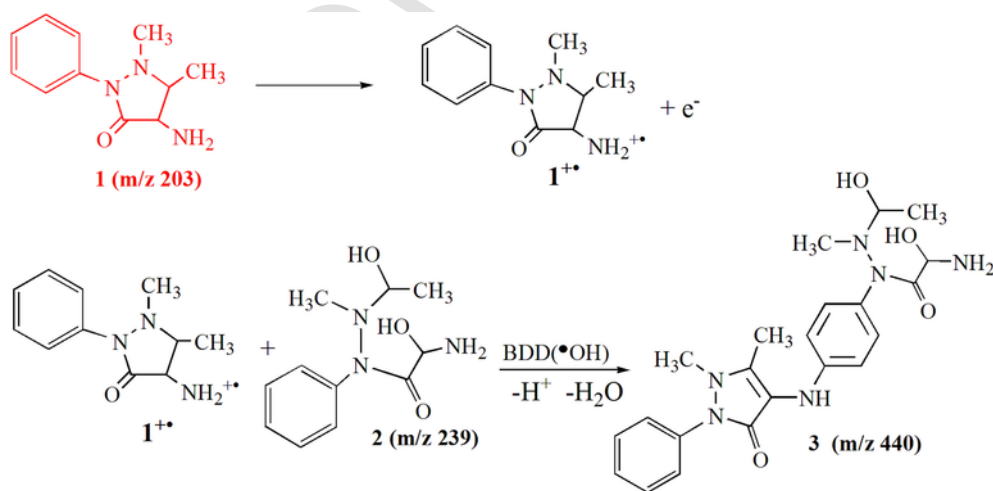

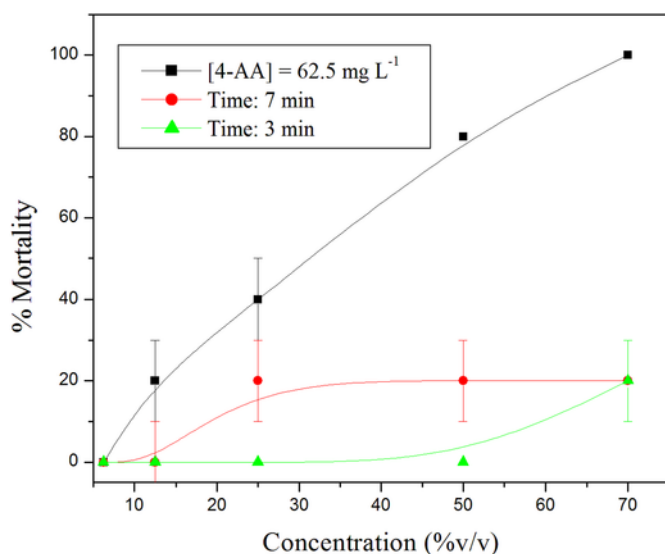**Fig. 6.** Proposed mechanism for the formation of the dimer intermediate.

Fig. 7. Change of *Artemia salina* mortality with the concentration of diluted aliquots of the initial $62.5\,mg\,L^{-1}$ 4-AA solution at pH = 3.5 and the remaining solutions after EO-H_2O_2 treatment at $j = 77.5\,mA\,cm^{-2}$ for 3 and 7 min.

on the percentage of mineralization and MCE. Optimum degradation conditions were obtained for $62.5\,mg\,L^{-1}$ drug solutions at pH = 3.5 and $j = 77.5\,mA\,cm^{-2}$, where 63% and 99% reduction were attained at 3 and 7 min, respectively. For the same kind of solutions, mineralization was optimum at $j = 77.5\,mA\,cm^{-2}$, with 45% TOC abatement in 175 min. Operating at $j = 77.5\,mA\,cm^{-2}$, an almost total mineralization with 91% TOC decay was found after 510 min. A complete initial reaction pathway for 4-AA degradation has been proposed, involving hydroxylated and carboxylic acid derivatives and one dimer. The treated solutions did not cause acute toxicity on *Artemia salina*, in contrast to parent 4-AA solutions. From these results, EO-H_2O_2 with a BDD/air-diffusion cell can be proposed as an effective treatment of wastewater containing this class of drugs.

Acknowledgements

References

APHA, 2012. Standard Methods for the Examination of Water and Wastewater, 22nd ed. American Public Health Association, New York.

Benito, A., Penadés, A., Lliberia, J.L., Gonzalez-Olmos, R., 2017. Degradation pathways of aniline in aqueous solutions during electro-oxidation with BDD electrodes and UV/H_2O_2 treatment. Chemosphere 166, 230–237.

Bezerra, M.A., Santelli, R.E., Oliveira, E.P., Villar, L.S., Escaleira, L.A., 2008. Response surface methodology (RSM) as a tool for optimization in analytical chemistry. Talanta 76, 965–977.

Boye, B., Michaud, P.A., Marselli, B., Dieng, M.M., Brillas, E., Comninellis, C., 2002. Anodic oxidation of 4-chlorophenoxyacetic acid on synthetic boron-doped diamond electrode. New Diamond Front. Carbon Technol. 12, 63–72.

Brereton, R.G., 2003. Chemometrics: Data Analysis for the Laboratory and Chemical Plant. Wiley, Chichester.

Brillas, E., Sirés, I., 2015. Electrochemical removal of pharmaceuticals from water streams: reactivity elucidation by mass spectrometry. TrAC Trends Anal. Chem. 70, 112–121.

Calza, P., Sakkas, V.A., Medana, C.A.D., Vlachou, A.D., Dal Bello, F., Albanis, T.A., 2013. Chemometric assessment and investigation of mechanism involved in photo-Fenton and TiO_2 photocatalytic degradation of the artificial sweetener sucralose in aqueous media. Appl. Catal. B Environ. 129, 71–79.

Campos-Mañas, M.C., Plaza-Bolaños, P., Sánchez-Pérez, J.A., Malato, S., Agüera, A., 2017. Fast determination of pesticides and other contaminants of emerging concern in treated wastewater using direct injection coupled to highly sensitive ultra-high performance liquid chromatography-tandem mass spectrometry. J. Chromatogr. A 1507, 84–94.

Cavalcante, R.P., Dantas, R.F., Wender, H., Bayarri, B., Gonzalez, O., Gimenez, J., Esplugas, S., Machulek, A.J., 2015. Photocatalytic treatment of metoprolol with B-doped TiO_2: effect of water matrix, toxicological evaluation and identification of intermediates. Appl. Catal. B Environ. 176–177, 173–182.

Cavalcante, R.P., Dantas, R.F., Bayarri, B., Gonzalez, O., Giménez, J., Esplugas, S., Machulek, A.J., 2016. Photocatalytic mechanism of metoprolol oxidation by photocatalysts TiO_2 and TiO_2 doped with 5% B: primary active species and intermediates. Appl. Catal. B Environ. 194, 111–122.

Coria, G., Sirés, I., Brillas, E., Nava, J.L., 2016. Influence of the anode material on the degradation of naproxen by Fenton-based electrochemical processes. Chem. Eng. J. 304, 817–825.

Da Silva, L.M., Cavalcante, R.P., Cunha, R.F., Gozzi, F., Dantas, R.F., Oliveira, S.C., Machulek, A.Jr, 2016. Tolfenamic acid degradation by direct photolysis and the UV-ABC/H_2O_2 process: factorial design, kinetics, identification of intermediates, and toxicity evaluation. Sci. Total Environ. 573, 518–531.

Ebele, A.J., Abou-Elwafa Abdallah, M., Harrad, S., 2017. Pharmaceuticals and personal care products (PPCPs) in the freshwater aquatic environment. Emerg. Contam. 3, 1–16.

El Fels, L., Hafidi, M., Ouhdouch, Y., 2016. Artemia salina as a new index for assessment of acute cytotoxicity during co-composting of sewage sludge and lignocellulose waste. Waste Manag. 50, 194–200.

Feng, L., Van Hullebusch, E.D., Rodrigo, M.A., Esposito, G., Oturan, M.A., 2013. Removal of residual anti-inflammatory and analgesic pharmaceuticals from aqueous systems by electrochemical advanced oxidation processes. A review. Chem. Eng. J. 228, 944–964.

Giri, A.S., Golder, A.K., 2015. Decomposition of drug mixture in Fenton and photo-Fenton processes: comparison to singly treatment, evolution of inorganic ions and toxicity assay. Chemosphere 127, 254–261.

Gligorovski, S., Strekowski, R., Barbati, S., Vione, D., 2015. Environmental implications of hydroxyl radicals (•OH). Chem. Rev. 115, 13051–13092.

Gómez, M.J., Sirtori, C., Mezcua, M., Fernández-Alba, A.R., Agüera, A., 2008. Photodegradation study of three dipyrone metabolites in various water systems: identification and toxicity of their photodegradation products. Water Res. 42, 2698–2706.

Gowda, J.I., Buddanavar, A.T., Nandibewoor, S.T., 2015. Fabrication of multiwalled carbon nanotube-surfactant modified sensor for the direct determination of toxic drug 4-aminoantipyrine. J. Pharm. Anal. 5, 231–238.

Guelfi, D.R.V., Gozzi, F., Sirés, I., Brillas, E., Machulek Jr, A., de Oliveira, S.C., 2017. Degradation of the insecticide propoxur by electrochemical advanced oxidation processes using a boron-doped diamond/air-diffusion cell. Environ. Sci. Pollut. Res. 24, 6083–6095.

Guinea, E., Brillas, E., Centellas, F., Cañizares, P., Rodrigo, M.A., Sáez, C., 2009. Oxidation of enrofloxacin with conductive-diamond electrochemical oxidation, ozonation and Fenton oxidation. A comparison. Water Res. 43, 2131–2138.

Hu, X., Yang, J., Yang, C., Zhang, J., 2010. UV/H_2O_2 degradation of 4-aminoantipyrine: a voltammetric study. Chem. Eng. J. 161, 68–72.

Kasiri, M.B., Khata, A.R., 2011. Photooxidative decolorization of two organic dyes with different chemical structures by UV/H_2O_2 process: experimental design. Desalination 270, 151–159.

Lanzalaco, S., Sirés, I., Sabatino, M.A., Dispenza, C., Scialdone, O., Galia, A., 2017. Synthesis of polymer nanogels by electro-Fenton process: investigation of the effect of main operation parameters. Electrochim. Acta 246, 812–822.

Li, D., Tong, H.-X., Zhang, L., 2013. Preparation of TiO_2/ITO film by liquid phase deposition and its photoelectrocatalytic activity for degradation of 4-aminoantipyrine. Trans. Nonferrous Metals Soc. China 23, 3306–3311.

Marković, M., Jović, M., Stanković, D., Kovačević, V., Roglić, G., Gojgić-Cvijović, G., Manojlović, D., 2015. Application of non-thermal plasma reactor and Fenton reaction for degradation of ibuprofen. Sci. Total Environ. 505, 1148–1155.

Marselli, B., Garcia-Gomez, J., Michaud, P.A., Rodrigo, M.A., Comninellis, C., 2003. Electrogeneration of hydroxyl radicals on boron-doped diamond electrodes. J. Electrochem. Soc. 150, D79–D83.

Miao, H.-F., Zhu, X.-W., Xu, D.-Y., Lu, M.-F., Huang, Z.-X., Ren, H.-Y., Ruan, W.-Q., 2015. Transformation of aminopyrine during ozonation: characteristics and pathways. Chem. Eng. J. 279, 156–165.

Miao, H.-F., Cao, M., Xu, D.-Y., Ren, H.-Y., Zhao, M.-X., Huang, Z.-X., Ruan, W.-Q., 2015. Degradation of phenazone in aqueous solution with ozone: influencing factors and degradation pathways. Chemosphere 119, 326–333.

Moreira, F.C., Garcia-Segura, S., Boaventura, R.A.R., Brillas, E., Vilar, V.J.P., 2014. Degradation of the antibiotic trimethoprim by electrochemical advanced oxidation processes using a carbon-PTFE air-diffusion cathode and a boron-doped diamond or platinum anode. Appl. Catal. B Environ. 160–161, 492–505.

Moreira, F.C., Boaventura, R.A.R., Brillas, E., Vilar, V.J.P., 2017. Electrochemical advanced oxidation processes: a review on their application to synthetic and real wastewaters. Appl. Catal. B Environ. 202, 217–261.

Muñoz, I., Rodríguez, A., Rosal, R., Fernández-Alba, A.R., 2009. Life cycle assessment of urban wastewater reuse with ozonation as tertiary treatment: a focus on toxicity-related impacts. Sci. Total Environ. 407, 1245–1256.

Nogueira, R.F.P., Oliveira, M.C., Paterlini, W.C., 2005. Simple and fast spectrophotometric determination of H_2O_2 in photo-Fenton reactions using metavanadate. Talanta 66, 86–91.

Özcan, A., Şahin, Y., Koparal, A.S., Oturan, M.A., 2008. Propham mineralization in aqueous medium by anodic oxidation using boron-doped diamond anode. Experimental parameters' influence on degradation kinetics and mineralization efficiency. Water Res. 42, 2889–2898.

Panizza, M., Cerisola, G., 2009. Direct and mediated anodic oxidation of organic pollutants. Chem. Rev. 109, 6541–6569.

Pérez-Estrada, L.A., Malato, S., Agüera, A., Fernández-Alba, A.R., 2007. Degradation of dipyrone and its main intermediates by solar AOPs: identification of intermediate products and toxicity assessment. Catal. Today 129, 207–214.

Persoone, G., Marsalek, B., Blinova, I., Torkokne, A., Zarina, D., Manusadzianas, L., Nalecz-Jawecki, G., Tofan, L., Stepanova, N., Tothova, L., Kolar, B., 2003. A practical and user-friendly toxicity classification system with microbiotests for natural waters and wastewaters. Environ. Toxicol. 18, 395–402.

Prieto-Rodríguez, L., Oller, I., Klamerth, N., Agüera, A., Rodríguez, E.M., Malato, S., 2013. Application of solar AOPs and ozonation for elimination of micropollutants in municipal wastewater treatment plant effluents. Water Res. 47, 1521–1528.

Rabaaoui, N., Saad, M.E.K., Moussaoui, Y., Allagui, M.S., Bedoui, A., Elaloui, E., 2013. Anodic oxidation of o-nitrophenol on BDD electrode: variable effects and mechanisms of degradation. J. Hazard. Mater. 250–251, 447–453.

Santos, P.M.P., Antunes, A.M.M., Noronha, J., Fernandes, E., Vieira, A.J.S.C., 2010. Scavenging activity of aminoantipyrines against hydroxyl radical. Eur. J. Med. Chem. 45, 2258–2264.

Savic, I.M., Savic Iva, M.M., Stojiljkovic, S.T., Gajic, D.G., 2014. Modeling and optimization of energy-efficient procedures for removing lead(II) and zinc(II) ions from aqueous solutions using the central composite design. Energy 77, 66–72.

Singh, B., Kumar, R., Ahuja, N., 2004. Optimizing drug delivery systems using systematic "Design of Experiments" part I: fundamental aspects. Crit. Rev. Ther. Drug Carrier Syst. 22, 27–105.

Sirés, I., Brillas, E., Oturan, M.A., Rodrigo, M.A., Panizza, M., 2014. Electrochemical advanced oxidation processes: today and tomorrow. A review. Environ. Sci. Pollut. Res. 21, 8336–8367.

Steter, J.R., Brillas, E., Sirés, I., 2016. On the selection of the anode material for the electrochemical removal of methylparaben from different aqueous media. Electrochim. Acta 222, 1464–1474.

Tay, K.S., Madehi, N., 2015. Ozonation of ofloxacin in water: by-products, degradation pathway and ecotoxicity assessment. Sci. Total Environ. 520, 23–31.

Thiam, A., Brillas, E., Centellas, F., Cabot, P.L., Sirés, I., 2015. Electrochemical reactivity of Ponceau 4R (food additive E124) in different electrolytes and batch cells. Electrochim. Acta 173, 523–533.

Thiam, A., Sirés, I., Garrido, J.A., Rodríguez, R.M., Brillas, E., 2015. Decolorization and mineralization of Allura Red AC aqueous solutions by electrochemical advanced oxidation processes. J. Hazard. Mater. 290, 34–42.